Global shifts in vegetation compositional resilience over the past 8,000 years

Mengna Liao[1], Kai Li[1], Chenzhi Li[2, 3], Ulrike Herzschuh[3], Jian Ni[1]

[1] *College of Life Sciences, Zhejiang Normal University, Jinhua 321004, China*

[2] *State Key Laboratory of Lake and Watershed Science for Water Security, Nanjing Institute of Geography and Limnology, Chinese Academy of Sciences, Nanjing 211135, China*

[3] *Polar Terrestrial Environmental Systems, Alfred Wegener Institute Helmholtz Centre for Polar and Marine Research, Potsdam 14473, Germany*

Corresponding authors. mnliao@zjnu.edu.cn (ML), likai@zjnu.edu.cn (KL)

Abstract

Vegetation resilience, the ability of ecosystems to resist and recover from environmental perturbations, is critical for sustaining biodiversity and ecosystem services. Yet, its long-term dynamics and drivers remain poorly resolved. Here, we assess continental-scale vegetation compositional resilience over the past 8,000 years using 482 fossil pollen records from all major landmasses except Antarctica. We apply a composite resilience index based on time-series properties of pollen assemblages and assessed its temporal trends and drivers. Our results reveal a persistent, millennia-scale decline in resilience, with the most pronounced shifts occurring since the late Holocene. While climate variability plays a role in contributing to this trend, anthropogenic land-use change, particularly the expansion of intensive agriculture since approximately 4 to 3 thousand years ago, emerges as the dominant global driver. Our study demonstrates the complexity of mechanisms driving long-term changes in vegetation compositional resilience over the past 8,000 years. Nevertheless, ecological attributes exert a substantial, and often predominant, influence on the long-term trajectories of continental-scale vegetation compositional resilience. These findings underscore the vulnerability of terrestrial vegetation to sustained human disturbance and highlight the importance of historical perspectives for predicting future ecological stability.

Main

Ongoing climate change and anthropogenic disturbances have profoundly affected the dynamical stability of terrestrial ecosystems, but our understanding of long-term vegetation stability—particularly in terms of composition—remains limited. The dynamical stability of ecosystems governs their responsiveness to environmental fluctuations and determines the reliability with which these natural resources sustain life-supporting services for society[1,2]. Resilience is one of the key properties that jointly define stability[3], which describes the capacity of a system to resist and recover from external perturbations[4]. Recent studies have demonstrated a widespread decline in vegetation resilience across many regions over the past decades[5-8], based on satellite-derived vegetation metrics, including Vegetation Optical Depth (VOD) and Normalized Difference Vegetation Index (NDVI). While these metrics serve as indicators of gross primary production[9] and vegetation greenness or canopy coverage[10], they poorly reflect vegetation composition, which is a critical dimension for understanding shifts in ecosystem structure and function disturbed by climate change and human activities.

Vegetation's response to climate change manifests across a range of timescales from hundreds to tens of thousands of years, potentially showing nonlinear characteristics or demonstrating temporal lags[11]. The limitations in data observation post significant challenges for

empirical data in detecting critical shifts in the resilience of vegetation composition and attributing these shifts. Fossil pollen records offer long-term perspectives for inferring past plant community properties and their dynamics across local, regional, and global scales spanning the last few centuries to millions of years[12,13]. By compiling pollen data, recent studies have revealed that vegetation composition has been transformed globally by climate changes and increasing human disturbances since the last glacial maximum[14,15]. Moreover, the rates of vegetation compositional change accelerated unprecedently during the late Holocene in both magnitude and extent[16]. Given the profound transformations of vegetation ecosystems caused by climate changes and, particularly, human disturbances, large-scale vegetation stability or resilience could have undergone significantly shifts during the Holocene. However, as of now, there is no evidence to support this hypothesis, nor has it been confirmed whether human disturbances play the crucial role in driving continental or global changes in vegetation compositional resilience.

Ecosystems not only make direct responses to external forcings but also possess inherent ecological feedbacks that enable them to mediate responses to exogenous stress, thereby sustaining the resilience of ecosystems[17,18]. The stabilizing effect of biodiversity (generally measured by species richness) has received the most extensive attention and discussion[19,20]. Most biodiversity–stability relationships involve some forms of compensatory dynamics or insurance effect, which require either asynchrony of species responses to environmental fluctuation or the presence of functionally redundant species with differing sensitivities to specific perturbations[20-22]. While this certainly appears to be the case at the community level in some ecosystems over relatively short ecological timescales spanning years to no longer than decades[23-25], these patterns may not generalize to larger spatial scales or longer temporal scales[26,27]. Other biological attributes, such as species evenness and spatial self-organization, regulate ecosystem resilience as well[28,29]. While, the applicability of these stability mechanisms to explaining long-term resilience trajectories in vegetation composition remains uncertain. This knowledge gap underscores an urgent need to extend current knowledge to broader spatial extents and longer temporal baselines, thereby aligning research scales with the operational dimensions of global biodiversity management and conservation strategies.

Here, we assessed continental-scale vegetation resilience over the past 8,000 years using fossil pollen sequences from the recently published global late Quaternary pollen dataset[30]. A total of 482 pollen records (Figure 1) were selected from all continents (Methods), with the exception of Antarctica. For each record, we calculated a composite resilience index (CRI) (Methods), where an increasing CRI trend indicates enhanced vegetation resilience. The estimated CRI sequences were aggregated by continent, and each continental CRI dataset was fitted using generalized additive models (GAMs). We then rigorously assessed the relative importance of abiotic (including climate variables and land-use change) and biotic factors (including taxonomic diversity indices and synchrony), as well as their direct and indirect effects on vegetation resilience, employing piecewise structural equation models (SEMs). Our findings reveal a long-term, millennia-scale decline in compositional vegetation resilience, primarily triggered by intensified human interference with terrestrial landscapes.

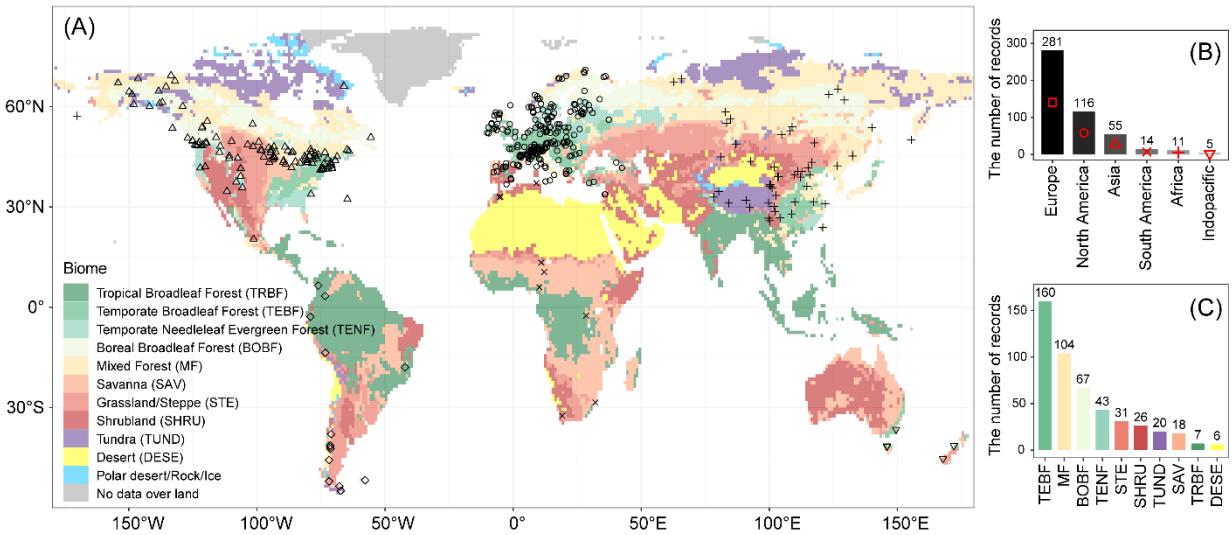

Figure 1. Spatial distribution of the fossil pollen sequences analyzed in this study, with sequence counts by continent and biome. (A) Spatial distribution of pollen sequences. (B) The number of pollen sequences per continent [symbols match those in (A)]. (C) The number of pollen sequences per biome [colors match those in (A)].

Results

All continents except Africa show significantly reversed CRI trends over the past 8,000 years (Figure 2). Notably, these reversed trends predominantly comprise a pattern of increase during the Mid-Holocene [8.0 to 4.2 thousand calibrated years before radiocarbon present (cal ka BP, where 0 ka BP is 1950 CE)], followed by a decline in the Late Holocene (4.2 to 0 cal ka BP), although the onset of these declines varied across continents (Figure 2). The earliest decline signal was detected in North America (4.4 cal ka BP), followed by Europe where the CRI began to decrease at 3.6 cal ka BP. For South America, Asia, and Oceania, the declines in CRI trends occurred at 2.8, 2.4, and 1.6 cal ka BP, respectively. Interestingly, in North America, the CRI trajectory over the past 1,200 years deviates from the “increase–decrease” pattern, showing an increasing trend instead.

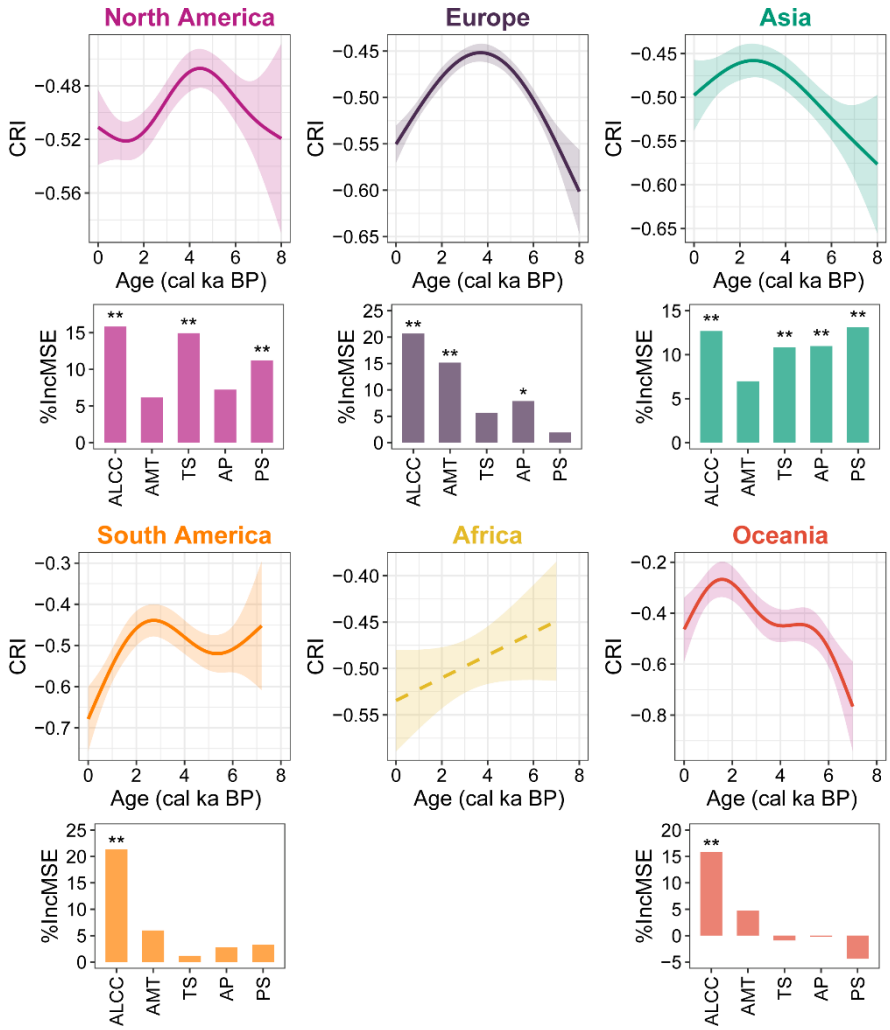

Figure 2. Continental CRI trends and relative importance of abiotic drivers. Solid lines denote significant fits ($P < 0.05$) of generalized additive model (GAM), while dashed lines indicate non-significant relationship ($P > 0.05$). The shaded areas represent the 95% confidential intervals of the GAM fits. Histograms show the relative importance of each driver, quantified as percentage increase in the mean squared error (%*InMSE*), with significant drivers marked with asterisks ($P < 0.05$ and ** $P < 0.01$). ALCC, anthropogenic land-cover change; AMT, annual mean temperature; TS, temperature seasonality; AP, annual precipitation; PS, precipitation seasonality.

The main abiotic predictors for the critical transitions in continental-scale CRIs were identified by random forest (RF) analysis (Figure 2, Methods). Anthropogenic land-cover change (ALCC) was the most important variable for predicting the critical transitions in the CRIs across all continents, except Asia where precipitation seasonality (PS) surpassed ALCC as the top-ranked driver. In addition to ALCC, the critical transition of CRIs in North America was significantly influenced by temperature seasonality (TS) and PS, whereas in the Europe it was significantly affected by annual mean temperature (AMT) and annual precipitation (AP). In Asia, both AP and TS showed comparable magnitudes of influence on the CRI transition.

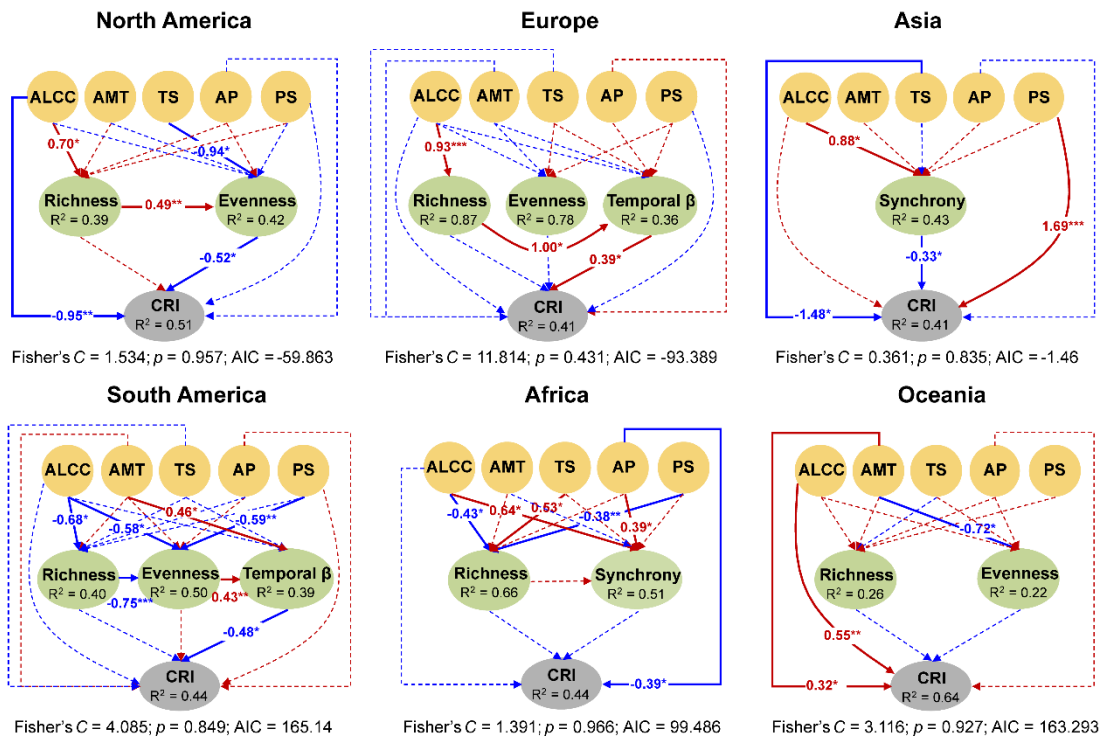

Figure 3. SEMs showing the direct and indirect effects of multiple abiotic and biotic drivers on CRI across six continents. Solid lines denote statistically significant paths ($P < 0.05$), while dashed lines indicate non-significant paths. Red and blue lines represent positive and negative effects, respectively. R^2 values indicate model-explained variance for each response variable. Standardized path coefficients are reported only for significant paths with significant level marked (* $P < 0.05$, ** $P < 0.01$, *** $P < 0.001$). Overall fit of SEM was evaluated using Shipley's test of d-separation: Fisher's C statistic (if $P > 0.05$, no paths are missing and the model is a good fit) and Akaike information criterion (AIC). ALCC, anthropogenic land-cover change; AMT, annual mean temperature; TS, temperature seasonality; AP, annual precipitation; PS, precipitation seasonality.

Pathways and effects of abiotic factors (AM, TS, AP, PS, ALCC) and ecological attributes (taxonomic richness, evenness, temporal β diversity, and synchrony) on CRIs have been estimated by Structure Equation Model (SEM) (Methods). In North America, the most prominent path is the direct link from ALCC to CRI. Evenness plays a significant role in influencing CRI, serving both as a significant direct driver to CRI variations and as a mediator that relays the effects of other factors to CRI. TS and richness have significant impacts on evenness, subsequently further affecting CRI. Moreover, ALCC exerts an indirect influence on CRI through richness (Figure 3). In Europe, temporal β diversity is the only factor that displays a significant direct path influencing the CRI. Richness shows a significant indirect path to CRI through temporal β diversity. ALCC exerts a substantial influence on richness, which subsequently further impacts CRI. In Asia, TS displays a strong positive direct path to CRI, while PS shows a strong negative direct path to CRI. Furthermore, synchrony exhibits a significant negative direct link to CRI, through which ALCC exerts negative effects on CRI. Similar to Europe, there are no significant direct paths from biotic factors to CRI, and temporal β diversity is the only factor that shows a significant direct path influencing CRI in South America. In this SEM, abiotic

factors contribute to CRI via several significant indirect paths, including those from AMT and evenness via temporal β diversity, from ALCC, PS, and richness via evenness, and from ALCC via richness. The SEM analysis for Africa reveals only one significant direct path originating from AP. Similar to Africa, the significant direct paths originate solely from abiotic factors in Oceania; however, the abiotic factors exerting significant impacts are ALCC and AMT, rather than AP.

The factors incorporated into the SEMs show varying effect sizes across different continents (Figure 4). In North America, evenness contributes most to CRI variations, with net effect size (*n.e.s.*, thereafter) of -0.7057. Although richness demonstrates both substantial positive and indirect negative effects on CRI, its net effect is weak. ALCC exerts a relatively strong effect on CRI in North America (*n.e.s.* = -0.1579), while other abiotic factors contribute comparatively minimal influence to CRI variation. In Europe, temporal β diversity (*n.e.s.* = 0.4274) emerges as the strongest driver of CRI variation, followed by evenness (*n.e.s.* = -0.3028). In Europe, the *n.e.s.* of richness on CRI is weak and ALCC is identified as the strongest abiotic driver of long-term CRI variation (*n.e.s.* = -0.2745). In Asia, PS (*n.e.s.* = 0.5886) and TS (*n.e.s.* = -0.54) show the notably stronger effects on CRI variation than all other evaluated factors. Synchrony also contributes a substantial effect on CRI (*n.e.s.* = -0.511). In South America, richness (*n.e.s.* = -0.5452) and temporal β diversity (*n.e.s* = -0.5142) are two strongest predictors of CRI variations, and AP (*n.e.s.* = 0.2169), ALCC (*n.e.s.* = -0.2023) and PS (*n.e.s.* = 0.1973) are the most important abiotic drivers. In Africa, richness (*n.e.s.* = 0.4255) and synchrony (*n.e.s.* = 0.3274) show obvious larger effect sizes on CRI variations than all other evaluated factors. Among abiotic factors, ALCC (*n.e.s.* = -0.1781) is the strongest predictor of CRI variation in Africa, following by AP (*n.e.s.* = -0.1563) and TS (*n.e.s.* = 0.1811). AMT (*n.e.s.* = 0.4119) and ALCC (*n.e.s.* = 0.3216) are the two most important factors influencing CRI in Oceania. Among biotic factors, the effect of evenness (*n.e.s.* = -0.3692) is stronger than that of richness (*n.e.s.* = -0.2069).

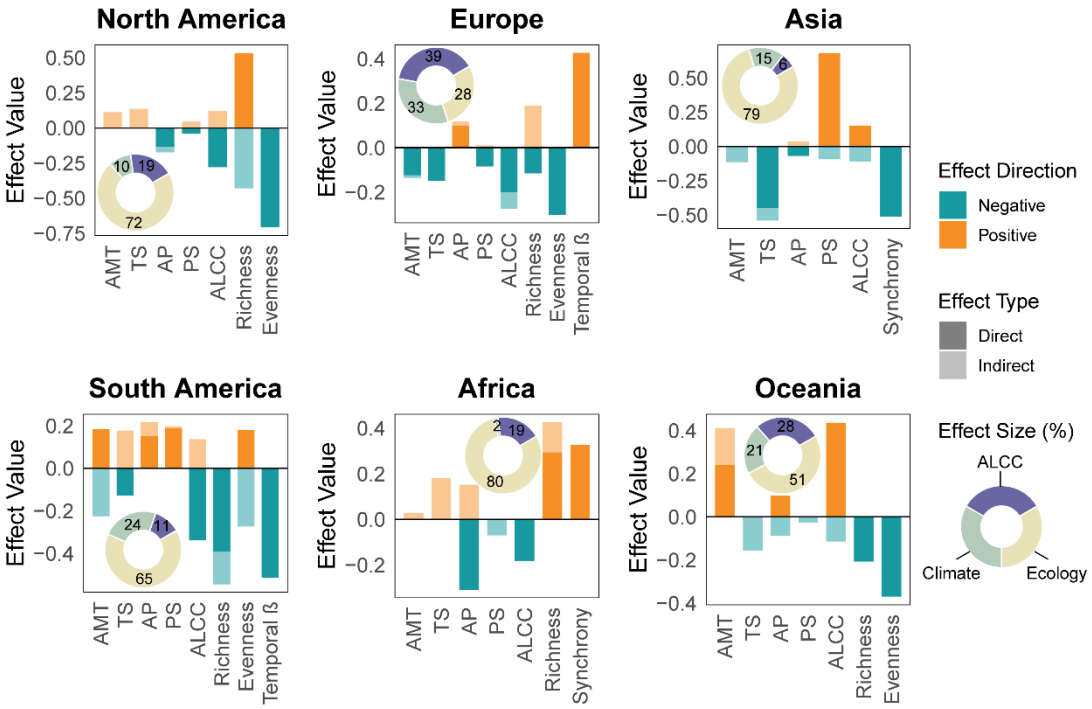

Figure 4. Effect sizes of abiotic and biotic drivers on continental CRI trajectories. Donut charts illustrate the relative net contribution of each grouped variable to continental CRI changes. ALCC, anthropogenic land-cover change; AMT, annual mean temperature; TS, temperature seasonality; AP, annual precipitation; PS, precipitation seasonality.

When quantifying the total net effects (Method), ecological attributes account for a predominant proportion of the total *n.e.s.*, ranging from *ca.* 51% to *ca.* 80%, across all continents except Europe (Figure 4). In Europe, the three contributors of ALCC, climate (*i.e.*, AMT, TS, AP, and PS), and ecological exhibit relatively comparable *n.e.s.*, with ALCC emerging as the most important factor. Although evenness and temporal β diversity have the largest *n.e.s.* among all evaluated factors in the SEM for Europe, their opposing effects diminish the overall impact of ecological attributes on CRI. A similar situation emerged in Asia, where PS and TS are the two most influential variables affecting CRI, yet their counteracting effects result in climate contributing only a minor portion of the total net effect on CRI. When comparing abiotic factors, climate exerts a notable stronger influence than ALCC on CRI variations in South America and Asia. Conversely, ALCC plays a more important role than climate in North America and Africa, while the *n.e.s.* of these two contributors are comparable in Europe and Oceania.

Discussion

Pollen archives have recorded the global shifts of vegetation compositional resilience during the Holocene, with the onsets of resilience declines occurred approximately between 4.4 and 1.6 cal ka BP across different continents (Figure 2). This aligns with that the Holocene Earth experienced significant vegetation changes, manifesting in multiple dimensions such as shifts in the compositional and structural in terrestrial vegetation[14], accelerated rates of compositional change[16], and alterations in floristic diversity[31]. The critical transitions in vegetation properties (*i.e.*, composition, structure, turnover rates, diversity, and resilience) were temporally asynchronous in many instances, giving rise to the notable but asynchronized resilience turnovers of terrestrial vegetation from different continents. Interestingly, the global resilience decline reversed in North America at *ca* 1.2 cal ka BP (Figure 2). This phenomenon was collectively attributed to the shifts in the resilience trajectories of steppe, tundra, and savanna biomes during the past 1,500 and 2,000 years, as well as the concurrent slowdown in the resilience loss in forest and shrubland in North America (Figure S1). On a global scale, compositional resilience in tundra and savanna ecosystems diverged from their preceding declining trajectories and initiated a recovery at around 3–2 cal ka BP (Figure S2). Thus, the continental-to-global scale shifts in vegetation resilience should be predominantly shaped by the integrated effects of different ecosystem responses to external stress, with such differential responses likely contingent upon the intrinsic properties of these ecosystems[32].

ALCC primary triggered the reversed trends of continental vegetation resilience during the late Holocene (Figure 2), particularly in South America and Oceania where ALCC emerged as the sole statistically significant predictor driving shifts in CRI trends. Although human modification on Earth's landscapes can be traced back to the Paleolithic era, its adverse effects on vegetation compositional resilience did not occur until the late Holocene. Among the diverse array of resource procurement and land management, intensive agriculture's high demand for resources and its continuous modification of land makes it the strongest force in changing the

Earth's landscapes. Intensive agriculture was prevalent only in a few regions with suitable climatic conditions until 4–3 cal ka BP, after which it began to spread more widely across the globe[33]. The rapid expansion of intensive agriculture has largely coincided with the decline in the compositional resilience of global vegetation, suggesting the existence of a land-use threshold inducing shifts in the trajectories of vegetation resilience. In addition to ALCC, climatic variables contributed substantially to the shifts in the long-term trends of vegetation resilience, particularly in North America, Europe, and Asia (Figure 2), suggesting that the observed resilience decline was commonly trigged by the synergistic effects of human disturbance and climate change.

Both theoretical and empirical researches have delved into how various features of ecosystems, such as complexity of ecosystems[34], biodiversity[32,35-37], species synchrony[28,38], species evenness[28,39], spatial self-organization[29,40], affect ecosystem stability/resilience. The relationship between biodiversity and stability has long been a contentious issue, primarily focused on the question of whether greater diversity (number of species) leads to less variability in communities. Our findings reveals that species richness can exert positive, negative, or negligible effects on vegetation resilience, at least in terms of vegetation composition, when assessed across continental scale and millennial timescales (Figure 3). This conclusion supports that a general conclusion about the diversity-stability cannot be anticipated[19], since external pressures often affect stability and diversity simultaneously. The stabilizing effects of biodiversity arise from species' asynchronous responses to environmental fluctuations, a phenomenon commonly referred as insurance effects[41,42]. However, species synchrony was identified as an important structural component of the SEMs only for Asia and Africa (Figure 3). In Asia, the SEM demonstrates a negative link between synchrony and vegetation compositional resilience, which appears to align with the insurance effect. In contrast, the SEM of Africa reveals a positive pathway between synchrony and resilience. Furthermore, we observe a positive richness-synchrony relationship in Africa, which appears to contradict the hypothesis that increased species richness would enhance the likelihood of a community containing species with differing responses to abiotic drivers or competition, thereby reducing synchrony[43]. However, the positive correlation between species richness and synchrony observed in this study aligns with findings from an empirical global assessment that examined how species richness and synchrony influence community stability[28]. These findings collectively suggest that the effect of richness on stability/resilience is not necessarily mediated through its negative influence on synchrony, either at the plot scale or at the continental scale.

Our study identifies evenness as another important direct or indirect predictor of long-term changes in vegetation compositional resilience across North and South America, Europe, and Oceania (Figure 3). Theoretically, declines in evenness may decrease temporal stability/resilience by weakening the portfolio effect or statistical averaging[44,45]. While, the SEMs predominantly reveal a negative association between evenness and resilience (Figure 3). This is likely because, akin to the mass-ratio hypothesis[46], dominant species exert stronger effect on vegetation dynamics than common and rare taxa do. When a vegetation ecosystem operates under a background where the dominant taxa progressively lose their ecological dominance (*i.e.*, evenness increase), a gradual decline of composition stability or resilience will arise from the reduced involvement of the dominants in shaping ecosystem structure and dynamics. Temporal β diversity, measuring changes in community composition or species assemblages over time at a

specific location[47], reflect species turnover and nestedness of assemblages, which result from species replacement and species loss or gain, respectively[48]. Here, temporal β diversity is calculated for adjacent time slices with a fixed interval, essentially serving as a metric for the rate of compositional change in an assemblage. It was expected that the variations in compositional change rates were expected to influence vegetation resilience, and this hypothesis is verified by the SEMs for Europe and South America (Figures 3 & 4). However, similar to species richness and evenness, the direction of temporal β diversity's impact on resilience is not fixed.

Despite these complexities present above, there are some general underlying mechanisms that drive changes in vegetation compositional resilience. Our study reveals that the assessed abiotic factors exert certain impacts on the biotic factors, and that some or all of these abiotic factors have direct influences on resilience (Figure 3). These findings emphasize that biotic factors unlikely change in isolation from abiotic drivers influencing stability, and in fact these abiotic drivers are typically the main causes of changes in ecological attributes and may serve as the original driving force for variations in ecosystem stability or resilience[19]. As another generality, both biotic and abiotic factors may have opposing effects on resilience through their direct and direct pathways (Figure 4). In some cases, a certain factor may appear to have a negligible impact on resilience because it simultaneously generates positive and negative effects of comparable magnitude. However, this does not necessarily imply that the positive and negative effects produced by this factor are weak *per se*. Regarding the relative importance of different factor types, biotic factors as a whole generally exert a substantially greater influence on continental-scale changes in compositional resilience than abiotic factors do, although Europe represents an exception to this pattern (Figure 4). Furthermore, while ALCC has been identified as the primary driver of the shift in the long-term trend of vegetation compositional resilience during the late Holocene, its cumulative effect on resilience trajectories over the past 8,000 years has not exceeded the cumulative influence of climate change across all continents.

Methods

Fossil pollen data source

Fossil pollen data are obtained from the LegacyPollen 2.0 dataset, a globally harmonized compilation of 3680 palynological records[49,50]. To ensure analytical consistency across diverse records, the dataset undergo rigorous taxonomic standardization—woody and dominant herbaceous taxa are harmonized at the genus level, while other herbaceous taxa are standardized at the family level[51]. Temporal standardization is achieved by constructing robust Bayesian age–depth models[30,52]. Each record contains both percentage and count data for identified taxa, along with calibrated age estimates corresponding to sediment depth.

Data filtering

We apply several criteria for data filtering, including archive type, the youngest and oldest depositional ages of records, the mean temporal resolution of samples, the total numbers of chronological control points, the presence or absence of sedimentary hiatus, and the temporal gap between adjacent samples. Firstly, we exclude records collected from marine, ice, and animal midden, as these archives rarely allow clear defining of the geographical source of fossil pollen. Regarding the depositional ages, we retain records with a minimal age no older than 2 cal ka BP and a basal age no younger than 10 cal ka BP. The adoption of this criterion ensures that the timeseries of the calculated vegetation resilience (see below for how CRI was calculated) spans

at least from the mid- to the late Holocene. We use a mean temporal resolution of 200 years as another data filtering criterion, based on a comprehensive assessment of both data availability and the capacity of pollen data to well resolve long-term vegetation dynamics over multi-millennial timescales. To minimize uncertainties arising from potential bias in estimated depositional ages, we exclude records containing fewer than three independent chronological control points from the analysis. The presence of pronounced sedimentary hiatus or large chronological gaps between adjacent samples in pollen records may result in either misinterpretation or failure to reconstruct vegetation dynamics accurately. Given this, we calculate the chronological gaps between each pair of adjacent samples in all records that met the aforementioned criteria. If a record contains a chronological gap exceeding 2,000 years, only its upper section is retained for subsequent analysis, contingent upon this section meeting the aforementioned criteria. Ultimately, we identify 482 pollen sequences that meet all the filtering criteria, including a total of 56,939 pollen samples. Among these sequences, 60.5% contain samples that predate the onset of the Holocene (11.7 cal ka BP), 19.7% extend back to 15 cal ka BP, and only 3.1% reach as far back as 20 cal ka BP (Figure S3).

Compositional resilience index (CRI)

Resilience reduction, which is often related to phenomena known in dynamical systems theory as "critical slowing down" or "flicking", can be quantitatively characterized by increases in variance, autocorrelation, and skewness of system state variables[53-55]. In addition, kurtosis quantifies the sharpness and tail-heaviness of the probability distribution, thereby providing a statistical measure to detect the increased presence of rare values in system variables emerging during "flickering" or under strong perturbations[56]. As different individual metric may have different predictive ability, combination of several indicators into a composite indicator is more reliable inferring resilience change than a single leading indicator[6,57-59]. Compositional resilience index (CRI) can be computed as the sum of the standardized differences of each employed resilience metric[57]. In this study, we apply four simple leading indicators of ecological resilience namely, autocorrelation at-lag-1 (AR1), standard deviation (SD), skewness (SK), and kurtosis (KURT), to compute CRI for each selected pollen record (Eqs. 1–9)[56,57].

$$AR1 = \frac{\sum_{t=1}^{n-1}(z_t-\mu)(z_{t+1}-\mu)}{\sigma_z^2} \tag{1}$$

$$SD = \frac{1}{n-1}\sum_{t=1}^{n}(z_t-\mu)^2 \tag{2}$$

$$SK = \frac{\frac{1}{n}\sum_{t=1}^{n}(z_t-\mu)^3}{\sqrt{\frac{1}{N}\sum_{t=1}^{n}(z_t-\mu)^2}} \tag{3}$$

$$KURT = \frac{\frac{1}{n}\sum_{t=1}^{n}(z_t-\mu)^4}{\left(\sqrt{\frac{1}{N}\sum_{t=1}^{n}(z_t-\mu)^2}\right)^2} \tag{4}$$

$$\widehat{AR1}_t = \frac{AR1_t-\overline{AR1}_{1:t}}{sd(AR1_{1:t})} \tag{5}$$

$$\widehat{SD}_t = \frac{SD_t-\overline{SD}_{1:t}}{sd(SD_{1:t})} \tag{6}$$

$$\widehat{SK}_t = \frac{SK_t-\overline{SK}_{1:t}}{sd(SK_{1:t})} \tag{7}$$

$$\widehat{KURT}_t = \frac{KURT_t-\overline{KURT}_{1:t}}{sd(KURT_{1:t})} \tag{8}$$

$$CRI_t = -(\widehat{AR1}_t + \widehat{SD}_t + \widehat{SK}_t + \widehat{KURT}_t) \tag{9}$$

where z_t is the subset of time-detrended ecological state series (i.e., scores of DCA1 in this study) within a sliding window; z_{t+1} is the first-order lag series; μ and σ_z^2 are the mean and variance of z_t, respectively. n is the size of the sliding window. $AR1_t$, SD_t, SK_t, $KURT_t$, and CRI_t are the *AR1*, *SD*, *SK*, *KURT*, and *CRI* at time t, respectively. $AR1_{1:t}$, $SD_{1:t}$, $SK_{1:t}$, and $KURT_{1:t}$ denote the timeseries of *AR1*, *SD*, *SK*, and *KURT* from times 1 to t, respectively. $\overline{AR1}_{1:t}$, $\overline{SD}_{1:t}$, $\overline{SK}_{1:t}$, and $\overline{KURT}_{1:t}$ are the mean values of *AR1*, *SD*, *SK*, *KURT*, and *CRI* from times 1 to t, respectively. $\widehat{AR1}_t$, $\widehat{SD}_t$, $\widehat{SK}_t$, and $\widehat{KURT}_t$ indicate the normalized *AR1*, *SD*, *SK*, and *KURT* at time t. Given that an increase in these leading indicators theoretically signifies a decline in system resilience, a rising in the composite index (calculated as the sum of standardized differences across all employed leading indicator) will similarly indicate reduced resilience[57]. To make the composite index more intuitively reflect the direction of resilience change, we define the CRI_t as the negative value of the summed standardized differences.

Given that these leading indicators are applicable exclusively to one-dimensional timeseries[4], we perform detrended correspondence analysis (DCA) using 'decorana' function from the 'vegan' package[60] to generate an aggregate measure reflecting the compositional state of multi-dimensional pollen assemblages. The first axis of DCA (hereafter DCA1), which generally captures the dominant gradient of compositional variation, is used as the aggregate measure for calculating the leading indicators. Additionally, an underlying assumption for applying these leading indicators is that the observations or timeseries must be equidistant. Therefore, we linearly interpolate the DCA1 scores at 200-year intervals (corresponding to the maximum mean temporal resolution of the samples) to generate equivalent timeseries[53]. Subsequently, we detrend the interpolated DCA1 scores using a locally weighted regression smoother (LOESS) to remove long-term trends. The residuals between interpolated and fitted values of DCA scores are then used to compute the leading indicators[54].

The choice of the rolling window size is critical for calculating leading indicators[53]. To determine the optimal window size, we estimate AR1, SD, SK, and KURT using rolling window sizes ranging from 10% to 80% of the timeseries length, incremented in steps of five data points. Trends in the leading indicators across different window sizes are quantified using the Kendall tau rank correlation coefficient. For each indicator, the optimal rolling window size is independently selected for individual DCA1 residual timeseries based on the maximum Kendall tau value. Given that the optimal rolling window sizes generally vary across the four leading indicators for each residual timeseries, the temporal coverage of the composite index is determined by the common overlapping period among all four indicators. Eventually, continental CRI sequences for North America, Europe, and Asia span the past 8,000 years, whereas those for South America, Africa, and Oceania cover the past 7,200 or 7,000 years (Figure S3).

Leading indicator calculations and trend estimations of statistical moments with different rolling window sizes are performed using functions 'genetic_ews' and 'sensitively_ews', respectively, in 'earlywarnings' package[56].

Richness and evenness

Richness is quantified as the effective number of taxa (*Hill* number of order $q = 0$) in each pollen assemblage, while evenness is measured by assessing the equality in the abundances of individual pollen types within the assemblage[61,62]. Given that empirical estimates of *Hill* numbers tend to be an increasing function of sampling effort or sample completeness[63], richness is determined by calculating the expected number of taxa in samples rarefied to an fixed size of

300 pollen grains. Evenness is estimated by using the modified *Hill*'s ratio (Eq. 10)[64]:

$$E = (N2 - 1)/(N1 - 1) \quad (10)$$

where E is evenness; $N1$ is the *Hill* number of order q = 1 (equivalent to the exponential of Shannon entropy or diversity measure), serving as an estimate of the number of abundant taxa in an assemblage; $N2$ is the *Hill* numbers of order q = 2 (equivalent to the inverse of Simpson's measure index of concentration), providing an estimate of the number of very abundant taxa in an assemblage. *Hill* numbers (q = 0, 1, 2) are calculated using 'iNEXT' function from the 'iNEXT' package[63,65]

Temporal β diversity

Temporal β diversity between temporally adjacent sample pairs within each pollen record is quantified using the Sørensen pair-wase dissimilarity, calculated via the 'beta.pair' function in the 'betapart' package[66]. To guarantee the accuracy of β diversity estimations along a temporal gradient, it is essential to maintain a uniform time interval between adjacent samples. For this, pollen data from each record are linearly interpolated to generate a dataset with evenly spaced interval prior to calculating temporal β diversity. Dataset interpolation is performed using the function 'interp.dataset' from the package 'rioja'[67], with an interpolated interval set to 200 years to match the temporal resolution used for computing the CRI. Given that the algorithm for calculating the Sørensen pair-wase dissimilarity is exclusively applicable to present/absent data, all non-zero values in the interpolated pollen dataset are converted to 1.

Synchrony

We define synchronay between two species or taxa as the extent of correlation in their abundances over a specified time period, with values ranging from +1 (perfect synchrony) to 0 (maximum asynchrony). For a multispecies community, community-wide synchrony can commonly be measured as the mean correlation between the abundance of each species versus the rest of the community[68] or the arithmetic mean correlation coefficient across all species pairs[69,70]. Given that pollen data are presented as either the percentage abundance of each taxon in samples or the grain count of each taxon within rarefied samples with equal size, it is inappropriate to apply Gross's synchrony metric[68], as the correlation between the percentage abundance or grain count of each taxon and the rest of the assemblage would exhibit perfect correlation. Therefore, we consider community-wide synchrony metric based on correlation coefficient across all species pairs to be a feasible approach for reflecting the overall synchrony in pollen assemblages. In this study, we develop a new measure of overall synchrony for pollen assemblages as Eq.11:

$$\eta_w = \sum_i w_{ij} \cdot \left| r(A_i, A_j) \right| \quad (11)$$

where η_w denotes the weighted synchrony index; A_i and A_j represent the timeseries of percentage abundance for taxon i and taxon j ($i \neq j$), respectively; r is the correlation coefficient between A_i and A_j, with a significant level < 0.05; w_{ij} is the sum of the mean percentage abundances of taxa i and j within an assemblage over the targeted period, namely the sum of the averages of A_i and A_j. We use Kendall's tau coefficient to quantified the correlations between paired taxa, and the significance of these correlations is evaluated using a two-tailed t-test. To obtain temporal trajectory of synchrony change, η_w is calculated within a five-point rolling window (1000 years) of the interpolated pollen dataset (200-year resolution).

Resilience trends at continental and biome scales

We model continental and biome CRIs against time with GAMs. GAMs are nonparametric

data-driven regression models, which are effective in assessing nonlinear relationships between response and predictor variables without any restrictive assumptions[71]. To facilitate model convergence, we standardize each CRI timeseries using z-score normalization, which involves subtracting the mean from each data point and then dividing by the standard deviation. The standardized CRI timeseries are subsequently aggregated into continental subsets and biome subsets according to their geological locations. The information on the continents where the pollen records are obtained is from the LegacyPollen2.0 dataset. The ISLSCP II Potential Natural Vegetation dataset, sourced from the Earthdata platform (https://www.earthdata.nasa.gov/) and comprising fifteen vegetation types, is applied as the reference for defining biome subsets. For each subset, we fit a GAM to the pooled standardized CRI values (hereafter, CRI_st) using the 'gam' function in the 'mgcv' package[72]. In this process, we estimate a smooth function representing the relationship between CRI_st and time, assuming a Gaussian distribution. When formulating GAM equation, we designate CRI_st as the response variable and use the age corresponding to each CRI_st value as the predictor variable. We incorporate a thin plate regression spline smoother into the formula, setting the smoothing basis dimension to five for representing the smooth term. Given the heterogeneity (*e.g.*, variations in environmental conditions, local ecological differences) across sampling sites from which pollen records were derived, we include a random effect of sampling sites into the model to provide a more realistic representation of the underlying data structure and yield more robust results. The significance of the GAMs is evaluated using the F statistic.

Investigating key drivers for continental resilience transitions

We use a random forest (RF) model to identify the primary driver(s) responsible for the transition of continental resilience from an increasing to a declining trend during the late Holocene. RF analysis is a flexible, non-parametric regression tool which can handle a large number of predictors even in small datasets with a low number of observations, and is suited to analyzing non-linear relationships and complex interactions[73]. To capture the states of resilience trends, we create a dummy variable based on the fitted continental-scale trends of CRI_st (Figure 2) prior to conducting the analysis. Specifically, we assign a value of 1 to periods showing an increasing trend and 0 to those showing a decreasing trend. It is worth noting that, given our focus on the increase-to-decline transition during the late Holocene, we exclude data from the dummy variable for two specific periods: (1) post-1.4 cal ka BP in North America, where trajectories deviated from the post-transition decline, and (2) pre-5.8 cal ka BP in South America, where trajectories deviated from the pre-transition increase (Figure 2). This approach allow us to eliminate potential bias in assessing the relative importance of predictors that may arise from the existence of other transitions in the CRI_st trends. Additionally, RF analysis is not applied to Africa due to the absence of a discernible transition in its CRI_st trend (Figure 2).

In RF models, we use the dummy variable representing the resilience state as the response variable. The predictor variables include AMT, TS, AP, and PS, which are derived from CHELSA-TraCE21k dataset[74], as well as anthropogenic land use, which is obtained from the KK10 dataset scenario of ALCC[75]. Based on the geographical coordinates of the pollen records, we extract timeseries data of the predictor variables for all pollen record from the two datasets using the function 'extract' from the package 'terra'[76]. The time slices for the extracted data are selected to match those of the CRI_st timeseries. To generate continental-scale timeseries for each predictor variable, we firstly standardize each predictor's timeseries using z-score

transformation and then partition the standardized timeseries into six continental subsets based on their geographical locations (Figure S4). For each predictor, continental-scale timeseries are generated by computing the median values across all time slices within each continental subset.

Variable importance is quantified by the increase in out-of-bag error when the values of the variable are randomly permuted [77]. We estimate the importance of predictor variables using the percentage increase in the mean squared error (%*InMSE*), where higher %*InMSE* values indicate greater variable importance[77]. The significance of each predictor is assessed with 1,000 permutations of the response variable. A predictor is considered statistically significant if the permutation-induced increase in *MSE* exceed the 95th percentile of the null distribution generated from these permutations. RF analyses and the permutation are conducted using the functions 'rfPermute' and 'importance' from the package 'rfPermute'[78].

Attributing long-term changes of continental resilience

We perform piecewise structural equation models (SEMs) based on a maximum likelihood method to test direct and indirect pathways of biotic and abiotic factors on continental-scale resilience of vegetation composition. SEM provides a way to test postulated relationships between causal and confounding variables and to disentangle their effects[79]. We construct an initial SEM including climatic variables (AMP, TS, AP, PS) and ALCC as observed variables, biotic attributes (richness, evenness, temporal β diversity, synchrony) as latent variables, and the CRI as the dependent variable. The initial structure contains all possible biotic and abiotic relationships with CRI, but do not define structural paths among latent variables. Standardized path coefficients are used to measure the direct and indirect effects of predictors[80]. We refine the model structure by adding potentially significant pathway(s) and/or removing those with extremely weak standardized path coefficient to improve the fit. The minimal and best model is selected based on the Akaike Information Criterion (AIC). Fisher's C test is conducted to assess the global goodness-of-fit of the models ($P \geq 0.05$ indicated reliable models). We conduct SEM analyses using the function 'psem' from the package 'piecewiseSEM'[81], performing separately for each continent to examine continental-specific causal relationships among variables. Following a similar data processing protocol to that used for RF analysis, we generate continental-scale timeseries for each variable through multi-step procedure involving standardization of data using z-score normalization, partitioning of standardized data into continental subsets, and calculating median values for each time slices within each subset (Figure S5).

In SEM, direct effects are measured as the standardized path coefficients between variables, while indirect effects are calculated as the product of direct path coefficients along a specific causal chain. We calculate the direct and indirect effects for each observed and laten variable, independent of the statistical significance of the path coefficient(s). The net effect of each variable is estimated by summing its direct and indirect effects. In addition, we classify the observed and laten variables into three types: climate, ALCC, and ecological attributes, to evaluate the relative contributions of different factor types on resilience. The net effects of each factor type are quantified as the sum of all direct and indirect effects of the variables grouped within that type. Then, we evaluate the relative effect sizes of distinct factor types for each continental-scale SEM. Effect size is defined as the absolute value of the net effect. The relative contributions of each factor type are quantified as the proportion (%) of its effect size relative to the total effect size across all factor types.

We perform all data manipulations and analyses using R[82]. All packages mentioned in this

study are software extensions to the R environment.

Data Availability and Code Availability

The LegacyPollen2.0 pollen dataset is openly available at https://doi.pangaea.de/10.1594/PANGAEA.965907. The ISLSCP II Potential Natural Vegetation dataset is openly available at https://www.earthdata.nasa.gov/. The CHELSA-TraCE21k climate data is openly available at https://chelsa-climate.org/chelsa-trace21k/. The KK10 Anthropogenic Land Cover data is openly available at https://doi.pangaea.de/10.1594/PANGAEA.871369.

All the R's packages mentioned in the main text are openly available at https://cran.r-project.org/.

References

1 Armsworth, P. R. & Roughgarden, J. E. The economic value of ecological stability. *Proceedings of the National Academy of Sciences* **100**, 7147-7151 (2003).

2 Watson, R. *et al.* Summary for policymakers of the global assessment report on biodiversity and ecosystem services of the Intergovernmental Science-Policy Platform on Biodiversity and Ecosystem Services. 22-47 (Bonn, Germany, 2019).

3 Van Meerbeek, K., Jucker, T. & Svenning, J. C. Unifying the concepts of stability and resilience in ecology. *Journal of Ecology* **109**, 3114-3132 (2021).

4 Dakos, V. & Kéfi, S. Ecological resilience: What to measure and how. *Environmental Research Letters* **17**, 043003 (2022).

5 Smith, T., Traxl, D. & Boers, N. Empirical evidence for recent global shifts in vegetation resilience. *Nature Climate Change* **12**, 477-484 (2022).

6 Feng, Y. *et al.* Reduced resilience of terrestrial ecosystems locally is not reflected on a global scale. *Communications Earth & Environment* **2**, 88 (2021).

7 Boulton, C. A., Lenton, T. M. & Boers, N. Pronounced loss of Amazon rainforest resilience since the early 2000s. *Nature Climate Change* **12**, 271-278 (2022).

8 Forzieri, G., Dakos, V., McDowell, N. G., Ramdane, A. & Cescatti, A. Emerging signals of declining forest resilience under climate change. *Nature* **608**, 534-539 (2022).

9 Liu, Y. Y. *et al.* Recent reversal in loss of global terrestrial biomass. *Nature Climate Change* **5**, 470-474 (2015).

10 Myneni, R. B., Keeling, C., Tucker, C. J., Asrar, G. & Nemani, R. R. Increased plant growth in the northern high latitudes from 1981 to 1991. *Nature* **386**, 698-702 (1997).

11 Fastovich, D. *et al.* Coupled, decoupled, and abrupt responses of vegetation to climate across timescales. *Science* **389**, 64-68 (2025).

12 Birks, H. J. B. Contributions of Quaternary botany to modern ecology and biogeography. *Plant Ecology & Diversity* **12**, 189-385 (2019).

13 Jackson, S. T. & Blois, J. L. Community ecology in a changing environment: Perspectives from the Quaternary. *Proceedings of the National Academy of Sciences* **112**, 4915-4921 (2015).

14 Nolan, C. *et al.* Past and future global transformation of terrestrial ecosystems under climate change. *Science* **361**, 920-923 (2018).

15 Gordon, J. D., Fagan, B., Milner, N. & Thomas, C. D. Floristic diversity and its relationships with human land use varied regionally during the Holocene. *Nature*

Ecology & Evolution, 1-13, doi:https://doi.org/10.1038/s41559-024-02457-x (2024).
16 Mottl, O. *et al.* Global acceleration in rates of vegetation change over the past 18,000 years. *Science* **372**, 860-864 (2021).
17 Blois, J. L., Zarnetske, P. L., Fitzpatrick, M. C. & Finnegan, S. Climate change and the past, present, and future of biotic interactions. *Science* **341**, 499-504 (2013).
18 Folke, C. *et al.* Regime shifts, resilience, and biodiversity in ecosystem management. *Annu. Rev. Ecol. Evol. Syst.* **35**, 557-581 (2004).
19 Ives, A. R. & Carpenter, S. R. Stability and diversity of ecosystems. *Science* **317**, 58-62 (2007).
20 Loreau, M. & De Mazancourt, C. Biodiversity and ecosystem stability: a synthesis of underlying mechanisms. *Ecology letters* **16**, 106-115 (2013).
21 de Bello, F. *et al.* Functional trait effects on ecosystem stability: assembling the jigsaw puzzle. *Trends in Ecology & Evolution* **36**, 822-836 (2021).
22 Oliver, T. H. *et al.* Biodiversity and resilience of ecosystem functions. *Trends in ecology & evolution* **30**, 673-684 (2015).
23 Isbell, F. *et al.* Biodiversity increases the resistance of ecosystem productivity to climate extremes. *Nature* **526**, 574-577 (2015).
24 Hisano, M., Searle, E. B. & Chen, H. Y. Biodiversity as a solution to mitigate climate change impacts on the functioning of forest ecosystems. *Biological Reviews* **93**, 439-456 (2018).
25 Hatton, I. A., Mazzarisi, O., Altieri, A. & Smerlak, M. Diversity begets stability: Sublinear growth and competitive coexistence across ecosystems. *Science* **383**, eadg8488 (2024).
26 Peterson, G., Allen, C. R. & Holling, C. S. Ecological resilience, biodiversity, and scale. *Ecosystems* **1**, 6-18 (1998).
27 Wang, S. & Loreau, M. Ecosystem stability in space: α, β and γ variability. *Ecology letters* **17**, 891-901 (2014).
28 Valencia, E. *et al.* Synchrony matters more than species richness in plant community stability at a global scale. *Proceedings of the National Academy of Sciences* **117**, 24345-24351 (2020).
29 Kéfi, S. *et al.* Self-organization as a mechanism of resilience in dryland ecosystems. *Proceedings of the National Academy of Sciences* **121**, e2305153121 (2024).
30 Li, C. *et al.* Harmonized chronologies of a global late Quaternary pollen dataset (LegacyAge 1.0). *Earth System Science Data* **14**, 1331-1343 (2022).
31 Gillson, L., MacPherson, A. J. & Hoffman, M. T. Contrasting mechanisms of resilience at mesic and semi-arid boundaries of fynbos, a mega-diverse heathland of South Africa. *Ecological Complexity* **42**, 100827 (2020).
32 Pennekamp, F. *et al.* Biodiversity increases and decreases ecosystem stability. *Nature* **563**, 109-112 (2018).
33 Stephens, L. *et al.* Archaeological assessment reveals Earth's early transformation through land use. *Science* **365**, 897-902 (2019).
34 Pimm, S. L. The complexity and stability of ecosystems. *Nature* **307**, 321-326 (1984).
35 Rodrigues, A. V. *et al.* Cross-Taxa Analysis of Long-Term Data Reveals a Positive Biodiversity-Stability Relationship With Taxon-Specific Mechanistic Underpinning.

Ecology Letters **28**, e70003 (2025).
36 Wang, S. & Loreau, M. Biodiversity and ecosystem stability across scales in metacommunities. *Ecology letters* **19**, 510-518 (2016).
37 Liang, M. *et al.* Unifying spatial scaling laws of biodiversity and ecosystem stability. *Science* **387**, eadl2373 (2025).
38 Schnabel, F. *et al.* Species richness stabilizes productivity via asynchrony and drought-tolerance diversity in a large-scale tree biodiversity experiment. *Science advances* **7**, eabk1643 (2021).
39 Isbell, F. I., Polley, H. W. & Wilsey, B. J. Biodiversity, productivity and the temporal stability of productivity: patterns and processes. *Ecology letters* **12**, 443-451 (2009).
40 De Paoli, H. *et al.* Behavioral self-organization underlies the resilience of a coastal ecosystem. *Proceedings of the national academy of sciences* **114**, 8035-8040 (2017).
41 Loreau, M. *et al.* Biodiversity as insurance: from concept to measurement and application. *Biological Reviews* **96**, 2333-2354 (2021).
42 Yachi, S. & Loreau, M. Biodiversity and ecosystem productivity in a fluctuating environment: the insurance hypothesis. *Proceedings of the National Academy of Sciences* **96**, 1463-1468 (1999).
43 McCann, K. S. The diversity–stability debate. *Nature* **405**, 228-233 (2000).
44 Hillebrand, H., Bennett, D. M. & Cadotte, M. W. Consequences of dominance: a review of evenness effects on local and regional ecosystem processes. *Ecology* **89**, 1510-1520 (2008).
45 Doak, D. F. *et al.* The statistical inevitability of stability-diversity relationships in community ecology. *The American Naturalist* **151**, 264-276 (1998).
46 Grime, J. Benefits of plant diversity to ecosystems: immediate, filter and founder effects. *Journal of Ecology* **86**, 902-910 (1998).
47 Magurran, A. E., Dornelas, M., Moyes, F. & Henderson, P. A. Temporal β diversity—A macroecological perspective. *Global Ecology and Biogeography* **28**, 1949-1960 (2019).
48 Baselga, A. Partitioning the turnover and nestedness components of beta diversity. *Global Ecology and Biogeography* **19**, 134-143 (2010).
49 Li, C. *et al.* LegacyPollen2. 0: an updated global taxonomically and temporally standardized fossil pollen dataset of 3680 palynological records, PANGAEA [data set bundled publication]. *PANGAEA–Data Publisher for Earth & Environmental Science* (2024).
50 Li, C. *et al.* Global biome changes over the last 21 000 years inferred from model–data comparisons. *Climate of the Past* **21**, 1001-1024 (2025).
51 Herzschuh, U. *et al.* LegacyPollen 1.0: a taxonomically harmonized global late Quaternary pollen dataset of 2831 records with standardized chronologies. *Earth System Science Data* **14**, 3213-3227 (2022).
52 Blaauw, M. & Christen, J. A. Flexible paleoclimate age-depth models using an autoregressive gamma process. (2011).
53 Dakos, V. *et al.* Slowing down as an early warning signal for abrupt climate change. *Proceedings of the National Academy of Sciences* **105**, 14308-14312 (2008).
54 Wang, R. *et al.* Flickering gives early warning signals of a critical transition to a

eutrophic lake state. *Nature* **492**, 419-422 (2012).

55 Scheffer, M. *et al*. Early-warning signals for critical transitions. *Nature* **461**, 53-59 (2009).

56 Dakos, V. *et al*. Methods for detecting early warnings of critical transitions in time series illustrated using simulated ecological data. *PloS one* **7**, e41010 (2012).

57 Drake, J. M. & Griffen, B. D. Early warning signals of extinction in deteriorating environments. *Nature* **467**, 456-459 (2010).

58 Su, H. *et al*. Long-term empirical evidence, early warning signals and multiple drivers of regime shifts in a lake ecosystem. *Journal of Ecology* **109**, 3182-3194 (2021).

59 Clements, C. F. & Ozgul, A. Including trait-based early warning signals helps predict population collapse. *Nature communications* **7**, 10984 (2016).

60 vegan: Community Ecology Package. R package version 2.6-4 (2022).

61 Birks, H. J. B. *et al.* Does pollen-assemblage richness reflect floristic richness? A review of recent developments and future challenges. *Review of Palaeobotany and Palynology* **228**, 1-25 (2016).

62 Hill, M. O. Diversity and evenness: a unifying notation and its consequences. *Ecology* **54**, 427-432, doi:doi:10.2307/1934352 (1973).

63 Chao, A. *et al*. Rarefaction and extrapolation with Hill numbers: a framework for sampling and estimation in species diversity studies. *Ecological Monographs* **84**, 45-67 (2014).

64 Alatalo, R. V. Problems in the measurement of evenness in ecology. *Oikos*, 199-204 (1981).

65 iNEXT: iNterpolation and Extrapolation for species diversity v. 3.0.0 (2022).

66 betapart: Partitioning Beta Diversity into Turnover and Nestedness Components. R package version 1.5.1 (2018).

67 rioja: Analysis of Quanternary Science Data, R package version (1.0-5) v. 1.0-5 (RCRAN, 2022).

68 Gross, K. *et al*. Species richness and the temporal stability of biomass production: a new analysis of recent biodiversity experiments. *The American Naturalist* **183**, 1-12 (2014).

69 Loreau, M. & de Mazancourt, C. Species synchrony and its drivers: neutral and nonneutral community dynamics in fluctuating environments. *The American Naturalist* **172**, E48-E66 (2008).

70 Thibaut, L. M. & Connolly, S. R. Understanding diversity–stability relationships: towards a unified model of portfolio effects. *Ecology letters* **16**, 140-150 (2013).

71 Hastie, T. & Tibshirani, R. Generalized additive models: some applications. *Journal of the American Statistical Association* **82**, 371-386, doi:https://doi.org/10.1080/01621459.1987.10478440 (1987).

72 Wood, S. N. Fast stable restricted maximum likelihood and marginal likelihood estimation of semiparametric generalized linear models. *Journal of the Royal Statistical Society Series B: Statistical Methodology* **73**, 3-36 (2011).

73 Feld, C. K., Segurado, P. & Gutierrez-Canovas, C. Analysing the impact of multiple stressors in aquatic biomonitoring data: A ‘cookbook’with applications in R. *Science of the Total Environment* **573**, 1320-1339 (2016).

74 Karger, D. N., Nobis, M. P., Normand, S., Graham, C. H. & Zimmermann, N. E. CHELSA-TraCE21k–high-resolution (1 km) downscaled transient temperature and precipitation data since the Last Glacial Maximum. *Climate of the Past* **19**, 439-456 (2023).

75 Kaplan, J. O. *et al*. Holocene carbon emissions as a result of anthropogenic land cover change. *The Holocene* **21**, 775-791 (2011).

76 terra: Spatial Data Analysis. R package version 1.7-29 v. 1.7-29 (RCRAN, 2023).

77 Breiman, L. Random forests. *Machine learning* **45**, 5-32 (2001).

78 rfPermute: Estimate Permutation p-Values for Random Forest Importance Metrics. R package version 2.5.2 v. 2.5.2 (RCRAN, 2023).

79 Shipley, B. *Cause and correlation in biology: A user's guide to path analysis, structural equations and causal inference with R (2nd edn)*. (Cambridge University Press, 2016).

80 Grace, J. B. & Bollen, K. A. Interpreting the results from multiple regression and structural equation models. *Bulletin of the Ecological Society of America* **86**, 283-295 (2005).

81 Lefcheck, J. S. piecewiseSEM: Piecewise structural equation modelling in r for ecology, evolution, and systematics. *Methods in Ecology and Evolution* **7**, 573-579 (2016).

82 R: A language and environment for statistical computing. R Foundation for Statistical Computing (Vienna, Austria, 2022).